Integrated Sensing and Communication Waveform Design With Sparse Vector Coding: Low Sidelobes and Ultra Reliability

Ruoyu Zhang, *Member, IEEE*, Byonghyo Shim, *Senior Member, IEEE*, Weijie Yuan, *Member, IEEE*, Marco Di Renzo, *Fellow, IEEE*, Xiaoyu Dang, and Wen Wu, *Senior Member, IEEE*

***Abstract*—Integrated sensing and communication (ISAC) can provide efficient usage for both spectrum and hardware resources. A critical challenge, however, is to design the dual-functional waveform for simultaneous radar sensing and communication. In this paper, we propose a sparse vector coding-based ISAC (SVC-ISAC) waveform to simultaneously provide low sidelobes for radar sensing and ultra reliability for communication transmission. The key idea of the proposed waveform is to embed the communication information into the support of one sparse vector and transmit a low-dimensional signal via the spreading codebook. We derive a closed-form expression of the ambiguity function for the proposed SVC-ISAC waveform, and prove that it exhibits low sidelobes in the delay and Doppler domains, regardless of the distribution of the transmitted bit stream. In addition, the information decoding at the communication receiver is solved through the support identification and sparse demapping. Simulation results demonstrate that the proposed waveform improves the reliability while consistently suppressing the sidelobe levels.**

***Index Terms*—Integrated sensing and communication, sparse vector coding, waveform design, ambiguity function, ultra reliability.**

I. Introduction

Integrated sensing and communication (ISAC), supporting both radar sensing and communication functionalities on a single platform and sharing the same frequency band, has been recognized as a promising technique for emerging applications, such as vehicle-to-everything (V2X), multi-function RF systems, unmanned aerial vehicle communication and sensing [1]–[3]. It is expected that such a technique can not only contribute to the efficient usage of spectrum and hardware resources, but also enable the cooperative design of radar and communications [3]–[5].

Manuscript received May 16, 2021; revised November 8, 2021; accepted January 15, 2022. Date of publication January 27, 2022; date of current version May 2, 2022. This work was supported in part by the Natural Science Foundation of Jiangsu Province under Grant BK20210335, in part by the National Natural Science Foundation of China under Grants 62031017, 61971221, and 62101232, in part by the MSIT (Ministry of Science and ICT), Korea, through the ITRC support program under Grant IITP-2021-0-02048, and in part by the NRF Grant funded by MSIP under Grant 2020R1A2C210198. The review of this article was coordinated by Prof. Yue Gao. *(Corresponding author: Weijie Yuan.)*

Ruoyu Zhang and Wen Wu are with the Ministerial Key Laboratory of JGMT, Nanjing University of Science and Technology, Nanjing 210094, China (e-mail: ryzhang19@njust.edu.cn; wuwen@njust.edu.cn).

Byonghyo Shim is with the Department of Electrical and Computer Engineering and the Institute of New Media and Communications, Seoul National University, Seoul 08826, South Korea (e-mail: bshim@snu.ac.kr).

Weijie Yuan is with the Department of Electrical and Electronic Engineering, Southern University of Science and Technology, Shenzhen 518055, China (e-mail: yuanwj@sustech.edu.cn).

Marco Di Renzo is with the Université Paris-Saclay, CNRS, CentraleSupélec, Laboratoire des Signaux et Systèmes, 91192 Gif-sur-Yvette, France (e-mail: marco.di-renzo@universite-paris-saclay.fr).

Xiaoyu Dang is with the College of Electronic and Information Engineering, Nanjing University of Aeronautics and Astronautics, Nanjing 211106, China (e-mail: dang@nuaa.edu.cn).

Digital Object Identifier 10.1109/TVT.2022.3146280

A central challenge is to design dual-functional waveforms that can simultaneously detect radar targets and transmit communication information [6]. Early works focused on embedding communication symbols into the radar waveform [7], [8]. In [7], the communication information was embedded into the intra or individual pulse of the incident radar waveform. In [8], the phases of the linear frequency modulation waveform for radar were used to represent the communications symbols. An alternative strategy of dual-functional waveform design is to tune widely used communication signals, e.g., orthogonal frequency division multiplexing (OFDM) for radar detection [9]–[11]. The work in [9] investigated the dynamic range and the resolution of OFDM signals, and developed a joint range and Doppler algorithm for radar target estimation. In [10], an OFDM waveform with a sufficient cyclic prefix was applied for synthetic aperture radar imaging. To make the most of spectrum resources, the authors of [11] proposed an adaptive OFDM-based joint radar and communications waveform design method under the total power constraint. In [12], a communication-embedded OFDM chirp waveform as well as its ambiguity function (AF) were investigated for the delay-Doppler radar. In [13], the applicability of phase modulated continuous waveform and OFDM was investigated in joint radar-communication systems, in which the normalized AF was computed to characterize the discrimination ability.

Another promising approach for ISAC waveform design is to utilize the index modulation (IM) technique [14]–[18]. In [15], the communication bits were represented by possible permutations of the orthogonal waveforms across transmitted antennas. Recently, as an advanced version of IM, a multi-carrier agile joint radar communication (MAJoRCom) system, integrating the carrier agile phased array radar, was proposed to enable the ISAC capability [16], [17]. In this scheme, the carrier frequencies over different pulse repetition periods can be randomly changed and allocated to antenna elements, and thus the agility in both spatial and frequency domains can be introduced. In [18], a generalized spatial modulation-based scheme was proposed to realize radar and communication functionalities, which improves communication rates by embedding additional data bits via the antenna selection.

While the goal of the aforementioned efforts is mainly on the design of dual-functional waveforms, the issue of sidelobe suppression has not been considered [19]–[21]. Due to the randomness of the embedded communication information, it is rather difficult to control the sidelobe level of the waveforms that are employed for ISAC. The authors of [22] employed a multiple-phase shift keying direct sequence spread spectrum signal, and developed a recursive least square filter to improve the radar peak sidelobe level. In [23], the weighted summation of communication and radar metrics under per-antenna power budget was considered, and the first-order descent algorithm was adopted to minimize the sidelobes. Nevertheless, the communication reliability, which is a crucial performance metric for many future applications such as autonomous driving and V2X [24], is not guaranteed in the aforementioned works. To the best of our knowledge, the design of ISAC waveforms that provide both low sidelobes and transmission reliability has not been investigated yet.

In this paper, we propose a sparse vector coding-based ISAC waveform (SVC-ISAC) to simultaneously achieve low sidelobes and ultra reliability. The key idea of the proposed SVC-ISAC waveform is to embed the communication information into the support of a sparse vector and then transmit the dimension-reduced signal via the spreading codebook. On this basis, we derive a closed-form expression of the

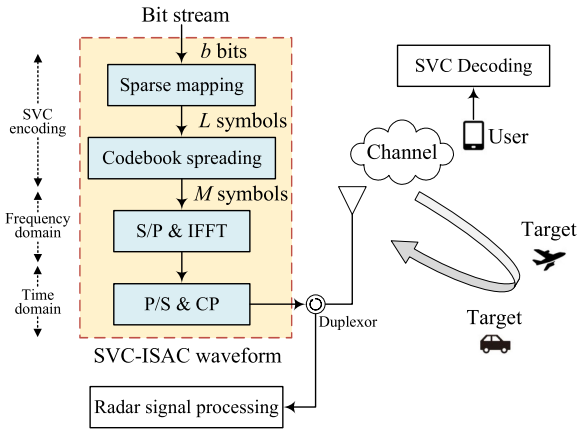

Fig. 1. The block diagram of the proposed SVC-ISAC waveform.

AF for the proposed SVC-ISAC waveform, and prove that it exhibits low sidelobes in the delay and Doppler domains, regardless of the probability distribution of the bit stream to be transmitted. Additionally, the information decoding at the communication receiver is performed via the support identification based on the sparse recovery and is followed by the sparse demapping. When compared to conventional IM-based signals, the proposed SVC-ISAC waveform is more flexible in the design of the index resources due to extra degrees of freedom provided by the spreading codebook. Simulation results demonstrate that the proposed SVC-ISAC waveform simultaneously achieves low sidelobes for radar sensing and ultra reliability for data transmission.

Notations: Vectors and matrices are denoted by lowercase and uppercase boldface letters, respectively. $|\Omega|$ denotes the cardinality of the set Ω. $\|\cdot\|_0$ and $\|\cdot\|_2$ denote the l_0 norm and the l_2 norm, respectively. The operations of transpose, conjugate, and conjugate transpose are denoted by $(\cdot)^T$, $(\cdot)^*$, and $(\cdot)^H$, respectively. $\mathbf{I}_M$ is the identity matrix with dimension $M \times M$, and $\mathrm{j} = \sqrt{-1}$ is an imaginary unit. $\mathbb{E}[\cdot]$ denotes the mathematical expectation, $\mathrm{sinc}(x) = \frac{\sin(\pi x)}{\pi x}$, and $[x]^+$ denotes the operation that returns the integer part of a real number x.

II. Proposed SVC-Based Integrated Sensing and Communication Waveform

A. Sparse Vector Coding

Let $\mathbf{w}$ be a b-bit information vector to be transmitted. The first step of SVC encoding is to map $\mathbf{w}$ to an L-dimensional sparse vector $\mathbf{s}$ with sparsity K (the number of nonzero elements in $\mathbf{s}$ is K) [25]. In the second step, each nonzero element in $\mathbf{s}$ is spread into M resources via the spreading sequence $\mathbf{c}_l \in \mathbb{C}^{M\times 1}$. The codebook matrix $\mathbf{C} = [\mathbf{c}_1, \ldots, \mathbf{c}_L]$ is designed such that $\mathbf{Cs}$ contains enough information to recover the sparse vector $\mathbf{s}$ [26]. The corresponding received vector $\mathbf{y}$ is

$$\mathbf{y} = \mathbf{HCs} + \mathbf{v}, \tag{1}$$

where $\mathbf{H}$ and $\mathbf{v}$ are the channel matrix and the additive white Gaussian noise (AWGN), respectively. The decoding of the information vector $\mathbf{w}$ is achieved by first identifying the nonzero positions in $\mathbf{s}$ and then applying the sparse demapping.

B. Proposed SVC-ISAC Waveform

Fig. 1 depicts the block diagram of the proposed SVC-ISAC waveform. We consider a bit stream $\mathcal{W} = \{0, 1\}$, where bit 1 and bit 0 are generated with probability p_1 and p_0 $(= 1 - p_1)$, respectively. The bits from $\mathcal{W}$ are divided into N groups, and each group constitutes a b-bit information vector $\mathbf{w}_n \in \mathbb{C}^{b\times 1}$. Let $\Pi_K(\cdot)$ be the SVC encoding operator that performs the sparse mapping. Then, we have

$$\mathbf{s}_n = \Pi_K(\mathbf{w}_n), \tag{2}$$

where the support set of the L-dimensional sparse vector $\mathbf{s}_n$ is $\Omega_n = \mathrm{supp}(\mathbf{s}_n) = \{l : s_{l,n} \neq 0, 1 \leq l \leq L\}$, $\|\mathbf{s}_n\|_0 = |\Omega_n| = K$, and the nonzero elements of $\mathbf{s}_n$ satisfy $\boldsymbol{\xi} = \mathbf{s}_{n,\Omega_n}$. By exploiting the predefined spreading codebook $\mathbf{C}_n$, we can obtain the dimension-reduced signal $\mathbf{a}_n \in \mathbb{C}^{M\times 1}$ as

$$\mathbf{a}_n = \mathbf{C}_n\mathbf{s}_n = \sum\nolimits_{l\in\Omega_n} \mathbf{c}_{n,l}s_l, \tag{3}$$

where $\mathbf{c}_{n,l}$ is the l-th column of $\mathbf{C}_n$. After an inverse fast Fourier transform (IFFT) operation and a cyclic prefix (CP) insertion, the ISAC waveform with SVC can be represented by

$$x_{\mathrm{svc}}(t) = \sum_{n=0}^{N-1}\sum_{m=0}^{M-1} a_{m,n}e^{\mathrm{j}2\pi m\Delta f(t-nT)}u\left(\frac{t-nT}{T}\right), \tag{4}$$

where $a_{m,n}$ is the m-th element of $\mathbf{a}_n$ in (3), Δf is the subcarrier spacing, $T = T_{\mathrm{eff}} + T_{\mathrm{CP}}$ is the duration of one OFDM symbol, where $T_{\mathrm{eff}} = 1/\Delta f$ and T_{CP} are the durations of the effective OFDM symbol and CP, respectively. The function $u(t)$ is the rectangular window, i.e., $u(t) = 1$, $t \in [0, T]$, otherwise $u(t) = 0$. From (2) to (4), we can encode $\lfloor \log_2 \binom{L}{K} \rfloor$ information bits within one OFDM symbol, and accordingly the spectral efficiency of the SVC-ISAC waveform is $\frac{\lfloor \log_2 \binom{L}{K} \rfloor}{MT\Delta f}$.

The benefits of the proposed SVC-ISAC waveform are threefold: 1) The support of the sparse vector is exploited for the information embedding, which is different from the conventional OFDM signal relying on the amplitudes and phases of constellation points to represent the data information. 2) The proposed SVC-ISAC waveform inherits the large time and bandwidth product of OFDM signals and is compatible with OFDM radar receivers [10], so the hardware complexity does not increase. 3) The proposed waveform intentionally constructs a high-dimensional sparse vector, which is capable of exploiting the transmission diversity and achieving ultra reliability.

It is worth pointing out that the spreading codebook $\mathbf{C}_n$ plays a key role in the proposed SVC-ISAC waveform. From the communication perspective, the dimension of the spreading codebook determines the occupied spectrum resources and the measurements for recovering the sparse vector $\mathbf{s}_n$, which affects the communication efficiency and reliability. In the radar sensing perspective, the spreading codebook directly generates $a_{m,n}$ onto multiple subcarriers, and accordingly affects the AF performance of the SVC-ISAC waveform.

III. Performance Analysis

In this section, we derive a closed-form expression of the AF for the proposed SVC-ISAC waveform and analyze its sidelobe performance in a statistical sense. We also discuss the communication receiver for the information decoding and the radar sensing receiver for the target estimation.

A. Ambiguity Function Analysis

The AF is one of the important tools to design and analyze the radar waveforms since it can fully characterize the radar discrimination capability in both range and velocity dimensions [19]. The definition of the AF for a signal $x(t)$ is given by

$$\chi(\tau, f_{\mathrm{d}}) = \int_{-\infty}^{+\infty} x(t)x^*(t-\tau)e^{\mathrm{j}2\pi f_{\mathrm{d}}t}\mathrm{d}t, \tag{5}$$

where τ and $f_{\rm d}$ are the time delay and the Doppler shift, respectively. By substituting (4) into (5), one can obtain the expression of the AF for the proposed SVC-ISAC waveform, as shown in (6) at the bottom of this page, where the terms γ, τ_1, τ_2, τ_3, and τ_4 are defined as

$$\gamma \triangleq \left[\frac{\tau}{T}\right]^+, -NT < \tau < NT, \tag{7}$$

$$\tau_1 \triangleq \tau + (1+|\gamma|)T, \tau_2 \triangleq \tau_1 - T, -NT < \tau < 0, \tag{8}$$

$$\tau_4 \triangleq \tau - (1+|\gamma|)T, \tau_3 \triangleq \tau_4 + T, 0 < \tau < NT. \tag{9}$$

In addition, $\chi^+_{n,n'}(\tau, f_{\rm d})$ in (10) and $\chi^-_{n,n'}(\tau, f_{\rm d})$ in (11) denote the cross AF between the n-th and n'-th symbols for the cases $0 < \tau < T$, and $-T < \tau < 0$, respectively. In the following, we provide a lemma describing the statistical behavior of the dimension-reduced signal $\mathbf{a}_n$.

$$\begin{aligned}\chi^+_{n,n'}(\tau, f_{\rm d}) = (T-\tau)&\sum_{m=0}^{M-1}\sum_{m'=0}^{M-1} a_{m,n}a^*_{m,'n'} \\ &\times e^{{\rm j}2\pi\left((m-m')\Delta f + f_{\rm d}\right)\frac{T+\tau}{2}} e^{{\rm j}2\pi m'\Delta f\tau} \\ &\times \operatorname{sinc}\left(\left((m-m')\Delta f + f_{\rm d}\right)(T-\tau)\right),\end{aligned} \tag{10}$$

$$\begin{aligned}\chi^-_{n,n'}(\tau, f_{\rm d}) = (T+\tau)&\sum_{m=0}^{M-1}\sum_{m'=0}^{M-1} a_{m,n}a^*_{m,'n'} \\ &\times e^{{\rm j}2\pi\left((m-m')\Delta f + f_{\rm d}\right)\frac{T+\tau}{2}} e^{{\rm j}2\pi m'\Delta f\tau} \\ &\times \operatorname{sinc}\left(\left((m-m')\Delta f + f_{\rm d}\right)(T+\tau)\right),\end{aligned} \tag{11}$$

Lemma 1: Regardless of the bit distribution p_0 or p_1, if the elements of the spreading codebook $\mathbf{C}_n$ and the nonzero elements $\boldsymbol{\xi}$ in the sparse vector $\mathbf{s}_n$ satisfy the conditions

$$p(c_{m,l,n} = 1) = p(c_{m,l,n} = -1) = 1/2, \tag{12}$$

and

$$\boldsymbol{\xi} = [1, \ldots, K/2, {\rm j}, \ldots, {\rm j}K/2]^T, \tag{13}$$

respectively, we have

$$\mathbb{E}\left[a_{m,n}a^*_{m,'n'}\right] = \begin{cases}\varepsilon, & m = m,' n = n,' \\ 0, & \text{otherwise},\end{cases} \tag{14}$$

for any positive even integer K, where ε is a constant.

Proof: See Appendix A. ■

Lemma 1 indicates that the transmit symbols of the proposed SVC-ISAC waveform exhibit the statistically orthogonal property in the frequency domain, and this statistical property is not related to the probability distribution of the input bit stream. With the aid of Lemma 1, we obtain the following theorem.

Theorem 1: The sidelobe of the AF for the proposed SVC-ISAC waveform satisfies

$$\mathbb{E}\left[\chi(\tau, f_{\rm d})\right] = \begin{cases}\psi\left(T - |\tau|\right)\operatorname{sinc}\left(f_{\rm d}(T-|\tau|)\right), & 0 < |\tau| < T, \\ 0, & |\tau| \geq T,\end{cases} \tag{15}$$

where $\psi = \varepsilon e^{{\rm j}\pi f_{\rm d}(T+\tau)}\sum_{n=0}^{N-1} e^{{\rm j}2\pi n f_{\rm d}T}\sum_{m=0}^{M-1} e^{{\rm j}2\pi m\Delta f\tau}$.

Proof: The range of the delay τ consists of two parts: $-NT < \tau < 0$ and $0 < \tau < NT$. We first consider the case $-NT < \tau < 0$, which can be further divided into two sub-cases. If the delay satisfies $-NT < \tau \leq -T$, i.e., $-N < \gamma \leq -1$, the expectation of the AF in (6) can be expressed as

$$\begin{aligned}\mathbb{E}\left[\chi(\tau, f_{\rm d})\right] = &\sum_{n=1}^{N-1+\gamma} e^{{\rm j}2\pi(n-1)f_{\rm d}T}\mathbb{E}\left[\chi^+_{n-1,n-\gamma}(\tau_1, f_{\rm d})\right] \\ &+ \sum_{n=0}^{N-1+\gamma} e^{{\rm j}2\pi n f_{\rm d}T}\mathbb{E}\left[\chi^-_{n,n-\gamma}(\tau_2, f_{\rm d})\right] = 0,\end{aligned} \tag{16}$$

where the last equality exploits Lemma 1, leading to the results of $\mathbb{E}[\chi^+_{n-1,n+|\gamma|}(\tau_1, f_{\rm d})] = 0$ and $\mathbb{E}[\chi^-_{n,n+|\gamma|}(\tau_2, f_{\rm d})] = 0$. If $-T < \tau < 0$, we have $\gamma = 0$. By exploiting Lemma 1, we have $\mathbb{E}[\chi^+_{n-1,n}(\tau_1, f_{\rm d})] = 0$, and thus (6) can be simplified to

$$\begin{aligned}\mathbb{E}\left[\chi(\tau, f_{\rm d})\right] &= \sum_{n=0}^{N-1} e^{{\rm j}2\pi n f_{\rm d}T}\mathbb{E}\left[\chi^-_{n,n}(\tau_2, f_{\rm d})\right] \\ &= (T+\tau)\varepsilon\sum_{n=0}^{N-1} e^{{\rm j}2\pi n f_{\rm d}T}\sum_{m=0}^{M-1} e^{{\rm j}\pi f_{\rm d}(T+\tau)} \\ &\quad\times e^{{\rm j}2\pi m\Delta f\tau}\operatorname{sinc}\left(f_{\rm d}(T+\tau)\right) \\ &= \psi(T+\tau)\operatorname{sinc}\left(f_{\rm d}(T+\tau)\right), -T < \tau < 0,\end{aligned} \tag{17}$$

where the second equality is derived from (8) since $\tau_2 = \tau + (1+|\gamma|)T - T = \tau$. The last equation is obtained by defining $\psi = \varepsilon e^{{\rm j}\pi f_{\rm d}(T+\tau)}\sum_{n=0}^{N-1} e^{{\rm j}2\pi n f_{\rm d}T}\sum_{m=0}^{M-1} e^{{\rm j}2\pi m\Delta f\tau}$.

The case $0 < \tau < NT$ can be analyzed in a similar way. If the delay satisfies $T \leq \tau < NT$, i.e., $1 \leq \gamma < N$, we have $\mathbb{E}[\chi^+_{n'+|\gamma|,n'}(\tau_3, f_{\rm d})] = 0$ and $\mathbb{E}[\chi^-_{n'+|\gamma|,n'-1}(\tau_4, f_{\rm d})] = 0$ with the aid of Lemma 1. Then, the expectation of the AF in (6) is 0. If $0 < \tau < T$, $\gamma = 0$, we obtain $\mathbb{E}[\chi^-_{n,'n'-1}(\tau_4, f_{\rm d})] = 0$ and the expectation of (6) becomes

$$\begin{aligned}\mathbb{E}\left[\chi(\tau, f_{\rm d})\right] &= \sum_{n'=0}^{N-1} e^{{\rm j}2\pi n' f_{\rm d}T}\mathbb{E}\left[\chi^+_{n,'n'}(\tau_3, f_{\rm d})\right] \\ &= (T-\tau)\varepsilon\sum_{n'=0}^{N-1} e^{{\rm j}2\pi n' f_{\rm d}T}\sum_{m=0}^{M-1} e^{{\rm j}\pi f_{\rm d}(T+\tau)} \\ &\quad\times e^{{\rm j}2\pi m\Delta f\tau}\operatorname{sinc}\left(f_{\rm d}(T-\tau)\right) \\ &= \psi(T-\tau)\operatorname{sinc}\left(f_{\rm d}(T-\tau)\right), 0 < \tau < T,\end{aligned} \tag{18}$$

where the second equality follows from $\tau_3 = \tau_4 + T = \tau - (1+|\gamma|)T + T = \tau$ in (9) and the last equality is from the definition of ψ. By combining (17) and (18), we obtain the desired result. ■

Theorem 1 reveals that the proposed SVC-ISAC waveform has low sidelobes in both delay and Doppler domains, irrespective of the input bit stream distribution. Accordingly, the proposed SVC-ISAC waveform exhibits the nearly ideal thumbtack-shape AF performance in a statistical sense, providing the capability to detect the targets with small radar cross section or in the nearby range-velocity bins.

B. Communication Receiver

In this subsection, we investigate the decoding strategy for the proposed SVC-ISAC waveform. After sampling with the sampling

$$\chi(\tau, f_{\rm d}) = \begin{cases}\sum_{n=1}^{N-1-|\gamma|} e^{{\rm j}2\pi(n-1)f_{\rm d}T}\chi^+_{n-1,n+|\gamma|}(\tau_1, f_{\rm d}) + \sum_{n=0}^{N-1-|\gamma|} e^{{\rm j}2\pi n f_{\rm d}T}\chi^-_{n,n+|\gamma|}(\tau_2, f_{\rm d}), & -NT < \tau < 0, \\ \sum_{n'=0}^{N-1-|\gamma|} e^{{\rm j}2\pi(|\gamma|+n')f_{\rm d}T}\chi^+_{n'+|\gamma|,n'}(\tau_3, f_{\rm d}) + \sum_{n'=1}^{N-1-|\gamma|} e^{{\rm j}2\pi(|\gamma|+n')f_{\rm d}T}\chi^-_{n'+|\gamma|,n'-1}(\tau_4, f_{\rm d}), & 0 < \tau < NT,\end{cases} \tag{6}$$

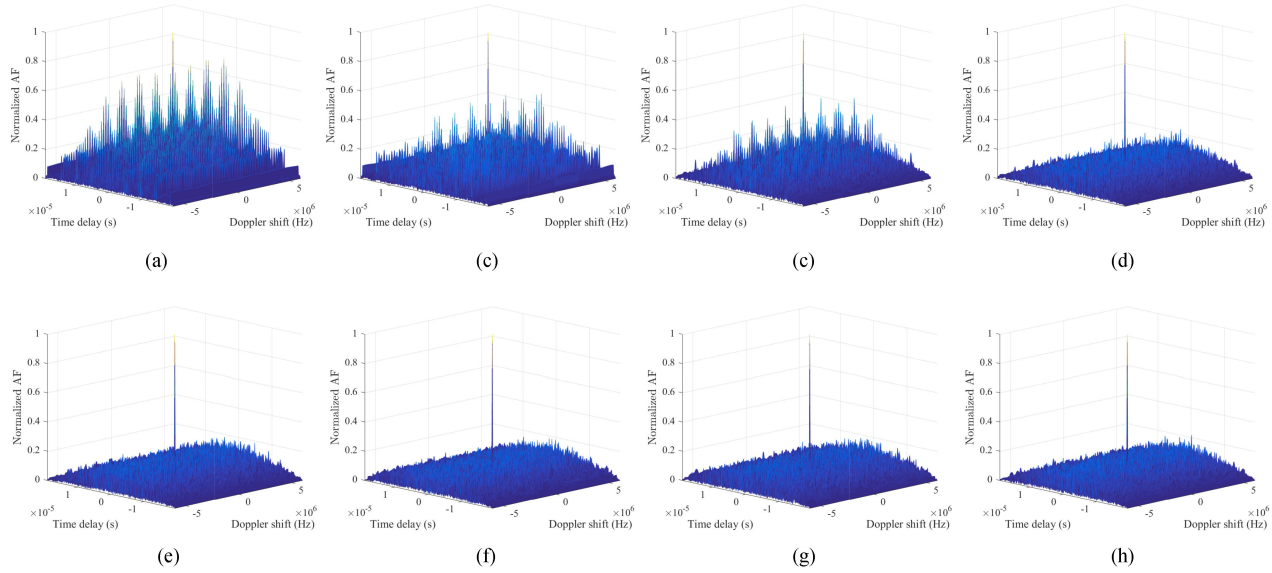

Fig. 2. Comparison of the normalized AF between the OFDM (upper row) and the proposed SVC-ISAC waveform (bottom row) under various bit distribution.

rate $f_s = M\Delta f$, removing the CP, and performing the discrete fourier transform (DFT), the received signal of the n-th SVC-ISAC symbol in the frequency domain can be represented by

$$\mathbf{y}_n = \mathbf{FHF}^H \mathbf{a}_n + \mathbf{v}_n, \tag{19}$$

where $\mathbf{y}_n$ is the received signal vector over M subscarriers, $\mathbf{F} \in \mathbb{C}^{M\times M}$ is the DFT matrix, $\mathbf{H} \in \mathbb{C}^{M\times M}$ is the circulant channel matrix whose first column is $\mathbf{h} = [h_0, h_1, \ldots, h_{P-1}, 0, \ldots, 0]^T$, and P is the number of channel taps ($N_{\mathrm{CP}} \geq P, N_{\mathrm{CP}} = \lceil T_{\mathrm{CP}} f_s \rceil$). The vector $\mathbf{v}_n \sim \mathcal{CN}(\mathbf{0}, \sigma^2 \mathbf{I}_M)$ denotes the AWGN of the communication link and the transmit power is denoted by $\rho = \mathbb{E}[|a_{m,n}|^2]$. In this setup, our goal is to identify the support set Ω_n corresponding to $\mathbf{a}_n$, rather than directly demodulating the frequency-domain signal $\mathbf{a}_n$. Relying on (3), we can formulate the SVC decoding as the following sparse signal recovery problem

$$\hat{\mathbf{s}}_n = \arg\min_{\mathbf{s}_n} \|\mathbf{y}_n - \mathbf{GC}_n\mathbf{s}_n\|_2 \ \text{ s.t. } \|\mathbf{s}_n\|_0 = K, \tag{20}$$

where $\mathbf{G} = \mathbf{FHF}^H$ is the frequency-domain channel matrix. After reconstructing the sparse signal, the support identification can be achieved by extracting the indices of the nonzero elements, i.e., $\hat{\Omega}_n = \mathrm{supp}(\hat{\mathbf{s}}_n)$. Since the sparsity K is also known to the communication receiver in advance, one can obtain the solution of $\mathbf{s}_n$ more accurately by using the sparsity-aware recovery techniques [27]. The information bits can be decoded via the sparse demapping $\Pi_K^{-1}(\cdot)$ based on the estimated $\hat{\Omega}_n$. It can be seen from (20) that no channel equalization is needed, which prevents the noise amplification in the zero-forcing method and the high complexity introduced by the minimum mean-squared error method.

C. Radar Sensing Receiver

For the functionality of radar sensing, the received echo signal of the transmitted SVC-ISAC waveform is expressed as

$$r(t) = \sum_{p=0}^{N_p-1} \sum_{q=1}^{Q} \beta_q x_{\mathrm{svc}}(t - \tau_q - pT_p) e^{\mathrm{j}2\pi \upsilon_q t} + w(t), \tag{21}$$

where Q is the number of targets, β_q, τ_q, and υ_q are the reflected coefficient, delay, and Doppler frequency of the q-th target, respectively, N_p is the number of transmitted pulses, T_p is the pulse repetition interval, $w(t)$ is the AWGN during the sensing process. The goal of radar sensing is to estimate the range and the velocity of targets, which can be addressed by the classic range-Doppler estimation method [19]. It should be noted that for the considered monostatic sensing system, the self-interference leaked from the continuously transmitted SVC-ISAC signal will saturate the receiver's amplifiers and will mask the echo signal containing the target information. Nevertheless, this issue has been treated in a recent work [28], in which the full-duplex techniques can be used for effectively detecting the target within the duration of a transmitted signal pulse.

IV. Simulation Results

In this section, we present numerical simulations to investigate the radar detection and communication reliability performance of the proposed SVC-ISAC waveform. The simulation parameters are as follows: $\Delta f = 240$ kHz, $M = 40$, $N = 4$, $L = 96$, $K = 2$, $T_{\mathrm{CP}} = 0.15T_{\mathrm{eff}}$. The bit 1 and bit 0 are generated with probabilities p_1 and p_0, respectively. Binary phase shift keying modulation is used in the conventional OFDM signal, while the elements of the spreading codebook $\mathbf{C}_n$ are generated from a Bernoulli distribution in the SVC-ISAC waveform.

As shown in Fig. 2, we first compare the normalized AF performance of the proposed SVC-ISAC waveform with that of a conventional OFDM signal when the probabilities p_1 and p_0 take different values. The normalized AF in Fig. 2 is calculated by $\frac{|\chi(\tau, f_{\mathrm{d}})|}{\max(|\chi(\tau, f_{\mathrm{d}})|)}$. When $p_1 = 0.1$, we see that the OFDM signal suffers from multiple spurious sidelobe peaks in terms of both the delay and Doppler domains, which results in a high miss and false detection probability. As the difference between p_1 and p_0 becomes smaller, the amplitude and quantity of spurious sidelobes gradually decrease. In contrast, the proposed SVC-ISAC waveform has a nearly ideal thumbtack-shape AF and exhibits low sidelobes in the delay and Doppler domains for any p_1 and p_0. This indicates that the proposed SVC-ISAC waveform consistently provides low sidelobes regardless of the distribution of transmitted information bits, which validates the theoretical analysis in Theorem 1.

We investigate the range-velocity estimation performance in Fig. 3, where the proposed SVC-ISAC, OFDM, and MAJoRCom waveforms are considered. The signal-to-noise ratio (SNR) of the radar sensing is

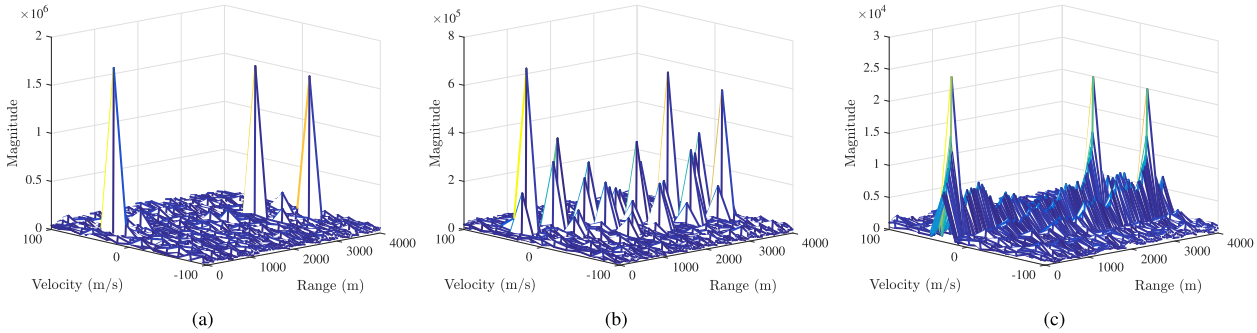

Fig. 3. Comparison of the range and velocity estimation for different waveforms.

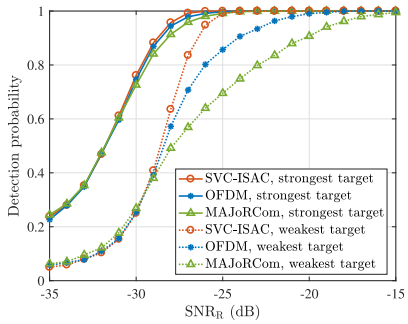

Fig. 4. Target detection performance versus $\mathrm{SNR_R}$.

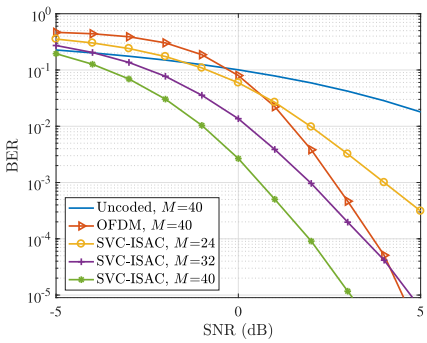

Fig. 5. BER performance as a function of SNR.

TABLE I
COMPARISON OF THE SPECTRAL EFFICIENCY (BITS/S/HZ)

Waveform	uncoded OFDM	coded OFDM	SVC-ISAC
$M = 24$	0.8	0.4	0.4
$M = 32$	0.8421	0.4211	0.3158
$M = 40$	0.8696	0.4348	0.2609

defined as $\mathrm{SNR_R} = 10\log\frac{\mathrm{E}[|\tilde{r}(t)|^2]}{\mathrm{E}[|w(t)|^2]}$, where $\tilde{r}(t)$ is the noiseless version of $r(t)$. The simulation setup is $f_c = 3\,\mathrm{GHz}$, $N_p = 64$, $T_p = 50\mu\mathrm{s}$, $Q = 3$, $\mathrm{SNR_R} = -10$ dB, $p_1 = 0.1$, the reflected coefficient, range, and velocity of 3 targets are (1, 200 m, 30 m/s), (0.9, 2900 m, 0 m/s), and (0.8, 3600 m, -30 m/s), respectively. From Fig. 3, it can be observed that, in the range-velocity plane, the OFDM signal suffers from multiple false peaks and the MAJoRCom waveform has rambling sidelobes alongside the peaks. In contrast, the proposed SVC-ISAC waveform exhibits no false peaks and low sidelobes, and three targets can be clearly distinguished. Under the same setting, the comparison of the target detection performance is shown in Fig. 4. We see that the proposed SVC-ISAC waveform achieves the best detection performance, especially for detecting the target with a small reflected coefficient.

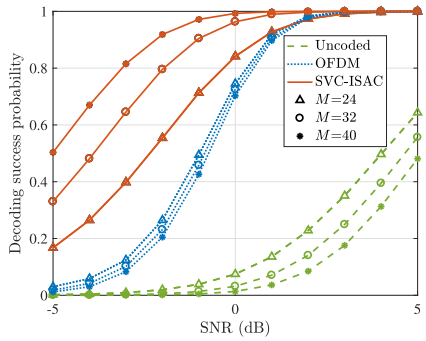

Fig. 6. Decoding success probability versus SNR.

The BER performance of the proposed SVC-ISAC waveform is depicted in Fig. 5, where both uncoded OFDM and coded OFDM (convolutional code with rate 1/2) systems are included for comparison. A frequency-selective fading channel with $P = 6$ taps and $||\mathbf{h}||_2^2 = 1$ is assumed, whose power delay profile is exponentially decaying. The successive interference cancellation-based matching pursuit algorithm in [27] is used to identify the support of the sparse signal in (20). The communication SNR is defined as $\mathrm{SNR} = 10\log\frac{\rho}{\sigma^2}$. We observe that the BER performance of the proposed SVC-ISAC waveform improves gradually with M, and the required SNR for achieving the BER of 10^{-5} is approximately 3 dB when $M = 40$. Compared to the classic coded OFDM systems, the communication system using the proposed SVC-ISAC waveform is capable of achieving an SNR gain of around 1.5 dB, at the cost of a spectral efficiency reduction from 0.4348 bits/s/Hz to 0.2609 bits/s/Hz.

The decoding success probability as a function of SNR is shown in Fig. 6, where the decoding is declared to be successful if the 0 and 1 bits in one OFDM symbol are all correctly demodulated. It can be seen that the decoding success probability of the conventional OFDM-based system gradually decreases with M. In contrast, the proposed SVC-ISAC waveform has the higher decoding performance, benefiting from the decreasing correlation of the spreading codewords as M increases. The spectral efficiencies for the different waveforms are listed in Table I. From Fig. 6 and Table I, we can see that under certain loss of the spectral efficiency, the proposed SVC-ISAC waveform achieves ultra reliable data transmission.

V. Conclusion

In this paper, we proposed the SVC-ISAC waveform by embedding the communication information into the support of the sparse vector and transmitting a low-dimensional signal using the spreading codebook. Due to the information embedding with the sparse mapping and codebook spreading, the proposed dual-functional waveform enhances the performances of both radar and communication. By analyzing a closed-form expression of the AF, we have proved that the proposed SVC-ISAC waveform exhibits a nearly ideal thumbtack-shape AF with low sidelobes in the delay and Doppler domains, regardless of the probability distribution of the input bit stream. By exploiting the support identification and the sparse demapping, we have shown that the proposed SVC-ISAC waveform achieves superior BER performance. Simulation results demonstrate the superiority of the proposed SVC-ISAC waveform in terms of radar discrimination capability and communication reliability.

Appendix A
Proof of Lemma 1

Proof: From (3), the m-th element of $\mathbf{a}_n$ is written as $a_{m,n} = \sum_{l\in\Omega_n} c_{m,l,n}s_{l,n}$. If $K=2$, i.e., $\boldsymbol{\xi}=[1,\mathrm{j}]^T$, the nonzero entries in $\mathbf{s}_n$ are only either 1 or j, regardless of the values of p_0 and p_1. Under the condition in (12), we obtain $p(a_{m,n}=1+\mathrm{j}) = p(a_{m,n}=1-\mathrm{j}) = p(a_{m,n}=-1+\mathrm{j}) = p(a_{m,n}=-1-\mathrm{j})$. Denote $a_{m,n}=\varrho e^{\mathrm{j}\vartheta}$, then $\mathbb{E}[a_{m,n}a^*_{m,'n'}] = \mathbb{E}[\varrho e^{\mathrm{j}\vartheta}\varrho e^{-\mathrm{j}\vartheta'}] = \varrho^2\mathbb{E}[e^{\mathrm{j}(\vartheta-\vartheta')}]$. We consider $\vartheta-\vartheta'$ as a random variable $\bar{\vartheta}\sim\bar{\boldsymbol{\vartheta}}$. If $\vartheta\neq\vartheta'$, the possible values of the random variable $\bar{\boldsymbol{\vartheta}}$ fall into the set $\{\pm\frac{\pi}{2},\pm\pi,\pm\frac{3\pi}{2}\}$. Thus, we have $\mathbb{E}[e^{\mathrm{j}(\vartheta-\vartheta')}] = \varphi(1) = \mathbb{E}[e^{\mathrm{j}\bar{\boldsymbol{\vartheta}}}] = \sum_{\bar{\vartheta}\in\bar{\boldsymbol{\vartheta}}} e^{\mathrm{j}\bar{\vartheta}}p(\bar{\boldsymbol{\vartheta}}=\bar{\vartheta}) = 0$. If $m=m,'n=n'$, i.e., $\vartheta=\vartheta'$, we have $\mathbb{E}[e^{\mathrm{j}(\vartheta-\vartheta')}] = \varphi(1) = \mathbb{E}[e^{\mathrm{j}\bar{\boldsymbol{\vartheta}}}] = p(\bar{\vartheta}=0)$. By defining the constant $\varepsilon \triangleq \varrho^2 p(\bar{\vartheta}=0)$, we obtain (14).

The case $K>2$ can be analyzed in a similar way. In this case, under the conditions in (12) and (13), we have $p(a_{m,n}=d_i)=\frac{1}{K^2}$, where $d_i\in\mathcal{D}$, $|\mathcal{D}|=K^2$, $i=1,\ldots,K^2$, $\mathcal{D}=\{1+\mathrm{j},1-\mathrm{j},\ldots,-\bar{K}-\mathrm{j}\bar{K}\}$, $\bar{K}\triangleq K/2$. By denoting $a_{m,n}=\varrho_i e^{\mathrm{j}\vartheta_i}$, we have $\mathbb{E}[a_{m,n}a^*_{m,'n'}] = \varrho_i\varrho_{i'}\mathbb{E}[e^{\mathrm{j}(\vartheta_i-\vartheta_{i'})}]$. Similarly, we consider $\vartheta_i-\vartheta_{i'}$ as a random variable $\bar{\boldsymbol{\vartheta}}_i$. Due to the equal probability of d_i, we have $\mathbb{E}[e^{\mathrm{j}(\vartheta_i-\vartheta_{i'})}] = \sum_{\bar{\vartheta}_i\in\bar{\boldsymbol{\vartheta}}_i} e^{\mathrm{j}\bar{\vartheta}_i}p(\bar{\boldsymbol{\vartheta}}_i=\bar{\vartheta}_i) = 0$ for $\vartheta_i\neq\vartheta_{i'}$. If $\vartheta_i=\vartheta_{i'}$, then $\mathbb{E}[a_{m,n}a^*_{m,'n'}] = \varrho_i\varrho_{i'}p(\bar{\vartheta}_i=0)$. By defining $\varepsilon\triangleq\varrho_i\varrho_{i'}p(\bar{\vartheta}_i=0)$, the proof is completed. ■

References

[1] P. Kumari, J. Choi, N. González-Prelcic, and R. W. Heath, "IEEE 802.11ad-based radar: An approach to joint vehicular communication-radar system," *IEEE Trans. Veh. Technol.*, vol. 67, no. 4, pp. 3012–3027, Apr. 2018.

[2] X. Chen, Z. Feng, Z. Wei, F. Gao, and X. Yuan, "Performance of joint sensing-communication cooperative sensing UAV network," *IEEE Trans. Veh. Technol.*, vol. 69, no. 12, pp. 15 545–15 556, Dec. 2020.

[3] F. Liu, C. Masouros, A. P. Petropulu, H. Griffiths, and L. Hanzo, "Joint radar and communication design: Applications, state-of-the-art, and the road ahead," *IEEE Trans. Commun.*, vol. 68, no. 6, pp. 3834–3862, Jan. 2020.

[4] L. Zheng, M. Lops, Y. C. Eldar, and X. Wang, "Radar and communication coexistence: An overview: A review of recent methods," *IEEE Signal Process. Mag.*, vol. 36, no. 5, pp. 85–99, Sep. 2019.

[5] D. Ma, N. Shlezinger, T. Huang, Y. Liu, and Y. C. Eldar, "Joint radar-communication strategies for autonomous vehicles: Combining two key automotive technologies," *IEEE Signal Process. Mag.*, vol. 37, no. 4, pp. 85–97, Jul. 2020.

[6] A. Hassanien, M. G. Amin, Y. D. Zhang, and F. Ahmad, "Signaling strategies for dual-function radar communications: An overview," *IEEE Aerosp. Electron. Syst. Mag.*, vol. 31, no. 10, pp. 36–45, Oct. 2016.

[7] S. D. Blunt, J. G. Metcalf, C. R. Biggs, and E. Perrins, "Performance characteristics and metrics for intra-pulse radar-embedded communication," *IEEE J. Sel. Areas Commun.*, vol. 29, no. 10, pp. 2057–2066, Dec. 2011.

[8] M. J. Nowak, Z. Zhang, L. LoMonte, M. Wicks, and Z. Wu, "Mixed-modulated linear frequency modulated radar-communications," *IET Radar Sonar Navig.*, vol. 11, no. 2, pp. 313–320, Dec. 2016.

[9] C. Sturm and W. Wiesbeck, "Waveform design and signal processing aspects for fusion of wireless communications and radar sensing," *Proc. IEEE*, vol. 99, no. 7, pp. 1236–1259, Jul. 2011.

[10] T. Zhang and X. Xia, "OFDM synthetic aperture radar imaging with sufficient cyclic prefix," *IEEE Trans. Geosci. Remote Sens.*, vol. 53, no. 1, pp. 394–404, Jan. 2015.

[11] Y. Liu, G. Liao, J. Xu, Z. Yang, and Y. Zhang, "Adaptive OFDM integrated radar and communications waveform design based on information theory," *IEEE Commun. Lett.*, vol. 21, no. 10, pp. 2174–2177, Oct. 2017.

[12] M. Li, W.-Q. Wang, and Z. Zheng, "Communication-embedded OFDM chirp waveform for delay-doppler radar," *IET Radar Sonar Navig.*, vol. 12, no. 3, pp. 353–360, Apr. 2017.

[13] S. H. Dokhanchi, B. S. Mysore, K. V. Mishra, and B. Ottersten, "A mmWave automotive joint radar-communications system," *IEEE Trans. Aerosp. Electron. Syst.*, vol. 55, no. 3, pp. 1241–1260, 2019.

[14] P. Yang, Y. Xiao, Y. L. Guan, M. Di Renzo, S. Li, and L. Hanzo, "Multidomain index modulation for vehicular and railway communications: A survey of novel techniques," *IEEE Veh. Technol. Mag.*, vol. 13, no. 3, pp. 124–134, Sep. 2018.

[15] E. BouDaher, A. Hassanien, E. Aboutanios, and M. G. Amin, "Towards a dual-function MIMO radar-communication system," in *Proc. IEEE Radar Conf.*, 2016, pp. 1–6.

[16] T. Huang, N. Shlezinger, X. Xu, D. Ma, Y. Liu, and Y. C. Eldar, "Multi-carrier agile phased array radar," *IEEE Trans. Signal Process.*, vol. 68, pp. 5706–5721, Aug. 2020.

[17] T. Huang, N. Shlezinger, X. Xu, Y. Liu, and Y. C. Eldar, "MAJoRCom: A dual-function radar communication system using index modulation," *IEEE Trans. Signal Process.*, vol. 68, pp. 3423–3438, May 2020.

[18] D. Ma *et al.*, "Spatial modulation for joint radar-communications systems: Design, analysis, and hardware prototype," *IEEE Trans. Veh. Technol.*, vol. 70, no. 3, pp. 2283–2298, Mar. 2021.

[19] M. A. Richards, *Fundamentals of Radar Signal Processing*, 2nd ed. New York, NY, USA: McGraw-Hill Education, 2005.

[20] G. Hua and S. S. Abeysekera, "Receiver design for range and doppler sidelobe suppression using MIMO and phased-array radar," *IEEE Trans. Signal Process.*, vol. 61, no. 6, pp. 1315–1326, Mar. 2013.

[21] J.-C. Chen, C.-K. Wen, and K.-K. Wong, "An efficient sensor-node selection algorithm for sidelobe control in collaborative beamforming," *IEEE Trans. Veh. Technol.*, vol. 65, no. 8, pp. 5984–5994, Aug. 2016.

[22] L. Tang, K. Zhang, H. Dai, P. Zhu, and Y.-C. Liang, "Analysis and optimization of ambiguity function in radar-communication integrated systems using MPSK-DSSS," *IEEE Wireless Commun. Lett.*, vol. 8, no. 6, pp. 1546–1549, Dec. 2019.

[23] F. Liu, C. Masouros, T. Ratnarajah, and A. Petropulu, "On range sidelobe reduction for dual-functional radar-communication waveforms," *IEEE Wireless Commun. Lett.*, vol. 9, no. 9, pp. 1572–1576, Sep. 2020.

[24] X. Ge, "Ultra-reliable low-latency communications in autonomous vehicular networks," *IEEE Trans. Veh. Technol.*, vol. 68, no. 5, pp. 5005–5016, May 2019.

[25] H. Ji, S. Park, and B. Shim, "Sparse vector coding for ultra reliable and low latency communications," *IEEE Trans. Wireless Commun.*, vol. 17, no. 10, pp. 6693–6706, Oct. 2018.

[26] W. Kim, S. K. Bandari, and B. Shim, "Enhanced sparse vector coding for ultra-reliable and low latency communications," *IEEE Trans. Veh. Technol.*, vol. 69, no. 5, pp. 5698–5702, Nov. 2020.

[27] R. Zhang, B. Shim, Y. Lou, S. Jia, and W. Wu, "Sparse vector coding aided ultra-reliable and low-latency communications in multi-user massive MIMO systems," *IEEE Trans. Veh. Technol.*, vol. 70, no. 1, pp. 1019–1024, Jan. 2021.

[28] C. B. Barneto, S. D. Liyanaarachchi, M. Heino, T. Riihonen, and M. Valkama, "Full duplex radio/radar technology: The enabler for advanced joint communication and sensing," *IEEE Wireless Commun.*, vol. 28, no. 1, pp. 82–88, Feb. 2021.